

# Signatures of Thermal Dilepton Radiation at RHIC

Ralf Rapp

*Department of Physics and Astronomy, State University of New York, Stony Brook, NY 11794-3800, U.S.A.*  
(October 27, 2018)

The properties of thermal dilepton production from heavy-ion collisions in the RHIC energy regime are evaluated for invariant masses ranging from 0.5 to 3 GeV. Using an expanding thermal fireball to model the evolution through both quark-gluon and hadronic phases various features of the spectra are addressed. In the low-mass region, due to an expected large background, the focus is on possible medium modifications of the narrow resonance structures from  $\omega$  and  $\phi$  mesons, whereas in the intermediate-mass region the old idea of identifying QGP radiation is reiterated including effects of chemical under-saturation in the early stages of central Au+Au collisions.

## I. INTRODUCTION

The identification of experimental signals from potential phase transitions in strong interaction matter associated with deconfinement and/or chiral symmetry restoration is the major goal of the (ultra-) relativistic heavy-ion program. Convincing evidence is likely to be achieved through a consistent combination of various suggested signatures. Among these is the copious production of thermal lepton pairs as originating from a supposedly thermalized fireball. Their relevance comes in two facets depending on invariant mass.

In the low-mass region (LMR, below  $\sim 1$  GeV) thermal radiation is governed by (in-medium) decays of the light vector mesons  $\rho$ ,  $\omega$  and  $\phi$ . With the dynamics in the light quark sector ( $u$ ,  $d$ ,  $s$ ) being driven by chiral symmetry and its spontaneous breaking in vacuum, medium modifications of the light vector mesons should encode information on (the approach to) chiral restoration. The challenge is then to discriminate the thermal contribution from the numerous 'background' mostly consisting of meson decays after freezeout of the interacting (hadronic) system.

At sufficiently high masses (above 3 GeV or so), primordial processes such as Drell-Yan annihilation (characterized by a much harder slope than typical thermal sources) or correlated decays of open anti-/charm (bottom) pairs are expected to prevail the spectra. Thus, the focus is on the narrow peaks from heavy vector mesons  $J/\Psi$ ,  $\Upsilon$ ,  $\dots$ , in connection with deconfinement signatures through their early dissolution. Descending from high masses thermal radiation is believed to become competitive below the  $J/\Psi$  resonance. In the so-called intermediate-mass region (IMR), extending down to the  $\phi$ , the emission is continuum-like with a magnitude approximately given by perturbative  $q\bar{q}$  annihilation. An enhanced dilepton yield in the IMR has been among the earliest suggestions [1] for a signal of QGP formation. The idea resides on the fact that at masses substantially larger than typical temperatures, thermal occupation factors strongly favor contributions from the hottest (early) stages of central collisions where deconfined, perturbative matter ought to be formed.

Dilepton measurements performed within the heavy-ion program at the CERN-SPS over the last decade have demonstrated that the above issues can be thoroughly addressed. For Sulfur and Lead projectiles both the LMR [2,3] and IMR [4,3] clearly exhibit appreciable signals above the aforementioned 'background' sources, *i.e.*, final state hadron decays as well as Drell-Yan and open charm contributions, respectively. At the same time extensive theoretical analyses have shown that the experimental findings can be consistently understood in terms of thermal emission (coupled with strong medium effects in the LMR, see, *e.g.*, ref. [5] for a recent review), indicating that one is indeed producing QCD matter in the vicinity of the conjectured phase boundary. Nevertheless, the major part of the enhancement is still associated with the hot and dense hadronic phases in the course of the collisions.

At the now operational collider experiments at RHIC, however, the plasma phase is anticipated to occupy much larger space-time volumes together with higher initial temperatures. At the same time, primordial and final hadron-decay sources increase. For the IMR various interplays have been elaborated in refs. [6–15], and for the LMR assessments have been made, *e.g.*, in ref. [16]. The purpose of the present article is to provide an overall picture as well as an improved estimate of the thermal component in both the IMR and LMR, thereby utilizing our understanding as inferred from the investigations performed in the context of the SpS results.

The article is organized as follows. In Sect. II we will recall basic ingredients for the description of equilibrium dilepton production rates from threshold to about 3 GeV. The emphasis will be on in-medium effects in the LMR, which will be assessed in the spectral function approach within hot hadronic matter as appropriate for RHIC conditions. In Sect. III we apply the emission rates using an expanding fireball model around midrapidity to calculate dilepton

invariant mass spectra, suitable for comparison with future measurements of the PHENIX detector. In the LMR special attention is paid to the manifestation of medium modifications of the light vector-meson resonances. In the IMR the predictions for thermal yields will be confronted with Drell-Yan pairs to evaluate their significance for identifying signals from an equilibrated partonic system. In particular, the consequences of chemical under-saturation in an early formed 'Gluon-Quark' Plasma will be assessed. In sect. IV we summarize and conclude.

## II. ELECTROMAGNETIC CORRELATION FUNCTION AND DILEPTON PRODUCTION RATES

### A. Definition and Spectral Decomposition

The general object for studying thermal dilepton emission is the electromagnetic (e.m.) current-current correlator [17,18]. In vacuum it is defined by the expectation value of the time-ordered product of e.m. currents,

$$\Pi_{\text{em}}^{\circ,\mu\nu}(q) = -i \int d^4x e^{iqx} \langle 0 | \mathcal{T} j_{\text{em}}(x) j_{\text{em}}(0) | 0 \rangle. \quad (1)$$

The correlation function provides a common framework not only for different hadronic approaches but also for quark-gluon based calculations. This feature is particularly evident in free space where the following decomposition of its imaginary part can be given:

$$\text{Im}\Pi_{\text{em}}^{\mu\nu} = \begin{cases} \sum_{V=\rho,\omega,\phi} ((m_V^{(0)})^2/g_V)^2 \text{Im}D_V^{\mu\nu}(M, \vec{q}; \mu_B, T) & , M \leq M_{\text{dual}} \\ (-g^{\mu\nu} + q^\mu q^\nu/M^2) (M^2/12\pi) N_c \sum_{q=u,d,s} (e_q)^2 & , M \geq M_{\text{dual}} . \end{cases} \quad (2)$$

From total  $e^+e^- \rightarrow \text{hadrons}$  cross section data it is well established that the low-mass part of the correlator can be accurately described by the light vector mesons within the Vector Dominance Model (VDM), whereas above a 'duality threshold' of about  $M_{\text{dual}} \simeq 1.5$  GeV free quark-antiquark states satisfactorily saturate the strength (within 20% or so).

The thermal dilepton production rate per unit 4-volume and 4-momentum is directly related to the (spin-averaged) imaginary part of the in-medium (retarded) e.m. correlator through

$$\begin{aligned} \frac{dR_{l^+l^-}}{d^4q} &= -2 f^B(q_0; T) L_{\mu\nu} \text{Im}\Pi_{\text{em}}^{\mu\nu} \\ &= -\frac{\alpha^2}{\pi^3 M^2} f^B(q_0; T) \text{Im}\Pi_{\text{em}}(q_0, \vec{q}; T, \mu_B) , \end{aligned} \quad (3)$$

where the lepton tensor  $L_{\mu\nu}$  encodes the propagation of a virtual photon and its subsequent decay into a pair of leptons.

### B. Medium Effects in the Low-Mass Region (LMR)

In the LMR medium effects arise from changes of the vector-meson spectral functions in hot hadronic matter. At RHIC energies, due to the low stopping of the interpenetrating nuclei, one would not expect baryons to play a significant role at central rapidities. However, even for a vanishing net baryon density this may not necessarily be true once accounting for thermal excitations of  $N\bar{N}$  pairs in connection with the rather strong meson-baryon interactions (as compared to the relatively weaker meson-induced interactions). In the following we will employ standard many-body techniques to implement (hadronic) selfenergy corrections into the propagation of the three light vector mesons  $\rho$ ,  $\omega$  and  $\phi$ .

#### 1. $\rho$ -Meson

For the  $\rho$ -meson propagator,

$$D_\rho(M, q; T) = \left[ M^2 - m_\rho^{(0)2} - \Sigma_{\rho\pi\pi} - \Sigma_{\rho M} - \Sigma_{\rho B} \right]^{-1} \quad (4)$$

an extensive literature about hadronic in-medium modifications has emerged over the last 10 years (see [5] for a recent review). Here, we incorporate finite temperature effects along the lines of ref. [22], where the total in-medium selfenergy has been obtained in terms of polarizations of its pion cloud as well as resonant interactions with surrounding pions, kaons and rho mesons,  $M = \pi, K, \bar{K}, \rho$ . In addition, modifications due to nucleons as well as the most abundant baryonic resonances ( $B = N, \Delta(1232), N(1440), N(1520)$ ) are included following refs. [23,24]. Since the  $\rho^0$ -meson is an eigenstate under antiparticle conjugation, it equally interacts with antibaryons, thereby effectively doubling the impact of the baryonic component for  $\mu_B$  close to zero. *E.g.*, at  $(T, \mu_B) = (180, 0)$  MeV one has  $\varrho_B = \varrho_{\bar{B}} \simeq 0.46\varrho_0$  which is appreciable (including all nonstrange resonances up to  $m_B = 1.7$  GeV as well as the lightest hyperons;  $\varrho_0 = 0.16 \text{ fm}^{-3}$  denotes ground state nuclear matter density).

## 2. $\omega$ – Meson

The same approach as for the  $\rho$  is now adopted for the  $\omega$  meson (see also refs. [19–21] for somewhat different treatments). First, its vacuum selfenergy is constructed from a combination of the direct  $\omega \rightarrow \rho\pi$  and the  $\omega \rightarrow 3\pi$  decays derived from the interaction vertices (isospin structures suppressed) [25,26]

$$\mathcal{L}_{\omega\rho\pi} = G_{\omega\rho\pi} \epsilon_{\mu\nu\sigma\tau} \omega^\mu \partial^\nu \rho^\sigma \partial^\tau \pi \quad (5)$$

$$\mathcal{L}_{\omega 3\pi} = G_{\omega 3\pi} \epsilon_{\mu\nu\sigma\tau} \omega^\mu \partial^\nu \pi \partial^\sigma \pi \partial^\tau \pi, \quad (6)$$

respectively.  $G_{\rho\pi\omega}$  is taken from ref. [22] which (together with a hadronic formfactor) gives the correct radiative decay width  $\Gamma_{\omega \rightarrow \pi\gamma}$  (using VDM) and about 50% of the full hadronic width.  $G_{3\pi}$  is then adjusted to reproduce the missing part. Medium effects in the  $\pi\rho$  cloud are introduced through thermal Bose enhancement factors (evaluated in the Matsubara framework) as well as the in-medium  $\rho$  spectral function from above, *i.e.*,

$$\Gamma_{\omega \rightarrow \rho\pi}(s) = \frac{2 G_{\omega\rho\pi}^2}{8\pi} \int_0^{M_{max}} \frac{MdM}{\pi} A_\rho(M) [1 + f^\pi(\omega_\pi) + f^\rho(\omega_\rho)] 2q_{cm}^3 F_{\omega\rho\pi}(q_{cm})^2 \quad (7)$$

$$\begin{aligned} \Gamma_{\omega \rightarrow 3\pi}(s) = \frac{9 G_{\omega 3\pi}^2}{192\pi^3} \int_{m_\pi}^{\omega_{1,max}} d\omega_1 \int_{m_\pi}^{\omega_{2,max}} d\omega_2 & \left[ 1 + \left\{ \sum_{i=0}^2 f^\pi(\omega_i) \right\} + f^\pi(\omega_0) \{ f^\pi(\omega_1) + f^\pi(\omega_2) \} + f^\pi(\omega_1) f^\pi(\omega_2) \right] \\ & \times \left[ p_1^2 p_2^2 - \frac{1}{4} (p_0^2 - p_1^2 - p_2^2) \right] F_{\omega 3\pi}(p_0, p_1, p_2)^2 \end{aligned} \quad (8)$$

with  $M_{max} = \sqrt{s} - m_\pi$ ,  $\omega_{1,max} = \sqrt{s} - 2m_\pi$  and  $\omega_{2,max} = \sqrt{s} - (\omega_1 + m_\pi)$  (dynamical modifications of the pion propagators are smaller and have been neglected). The  $\omega$  can also be absorbed through the inelastic reaction  $\omega\pi \rightarrow \pi\pi$ . The corresponding collisional broadening has been calculated in ref. [20] which we include via

$$\Gamma_{\omega\pi \rightarrow \pi\pi} \simeq (7 \text{ MeV}) \left( \frac{T}{T_0} \right)^3 \quad (9)$$

( $T_0 = 150$  MeV). We furthermore compute an  $\omega$ -selfenergy from scattering off thermal pions inducing  $b_1(1235)$  resonance formation [19,20], which has the largest known coupling to  $\omega\pi$  states. Using the interaction vertex

$$\mathcal{L}_{\omega\pi b_1} = G_{\omega\pi b_1} b^\mu (g_{\mu\nu} p \cdot q - q_\mu p_\nu) \omega^\nu \pi, \quad (10)$$

the selfenergy takes the form

$$\Sigma_{\omega\pi b_1}(M, q) = G_{\omega\pi b_1}^2 \int \frac{p^2 dp dx}{(2\pi)^2 2\omega_\pi(p)} [f^\pi(\omega_\pi(p)) - f^{b_1}(q_0 + \omega_\pi(p))] F_{\omega\pi b_1}(q_{cm})^2 D_{b_1}(s) v_{\omega\pi b_1}(p, q), \quad (11)$$

where the vertex function  $v_{\omega\pi b_1}(p, q)$  and the hadronic (dipole) formfactor  $F_{\omega\pi b_1}$  are in close analogy to the  $\rho\pi a_1$  case [22]. The coupling constant and cutoff parameter are fitted to the empirical hadronic and radiative decay widths  $\Gamma_{b_1 \rightarrow \pi\omega, \pi\gamma}$ .

In nuclear matter, according to the coupled channel analysis for vector meson-nucleon scattering of ref. [30], the dominant coupling of the  $\omega$  proceeds through resonant  $N(1520)N^{-1}$  excitations (with a strength similar to that for the  $\rho$  meson), as well as  $N(1650)N^{-1}$  ones. Modifications induced in the pion cloud are presumably less significant [31],

especially when using soft formfactors for the  $\pi NN$  and  $\pi N\Delta$  as suggested by the analysis of photoabsorption spectra on the nucleon and nuclei [32]. In line with the arguments given above (see also ref. [24]), we evaluate the  $N(1520)N^{-1}$  and  $N(1650)N^{-1}$  loops at an effective nucleon density

$$\varrho_{eff} = \varrho_N + \varrho_{\bar{N}} + 0.5 (\varrho_B + \varrho_{\bar{B}}) \quad (12)$$

to account for the effects of higher resonances as well as antibaryons. The in-medium  $\omega$  propagator finally reads

$$D_\omega = [M^2 - m_\omega^2 + im_\omega(\Gamma_{3\pi} + \Gamma_{\rho\pi} + \Gamma_{\omega\pi\rightarrow\pi\pi}) - \Sigma_{\omega\pi b_1} - \Sigma_{\omega B}]^{-1} . \quad (13)$$

### 3. $\phi$ -Meson

For the  $\phi$  meson various evaluations of medium effects based on hadronic rescatterings at finite temperature have indicated quite moderate changes of both its mass and width [27,28,20,29]. This also holds true for direct  $\phi N$  interactions as indicated by photonuclear production of  $\phi$  mesons as well as the absence of baryonic resonances with explicitly measured  $\phi N$  decay channels<sup>1</sup>. Therefore we do not attempt a microscopic description of this part of the  $\phi$  selfenergy but merely parameterize the finite-temperature collisional broadening guided by the results of ref. [20] as

$$\text{Im } \Sigma_\phi^{coll}(T) = -m_\phi \Gamma_\phi^{coll}(T_0) \left(\frac{T}{T_0}\right)^3 \quad (14)$$

with  $T_0 = 150$  MeV,  $\Gamma_\phi^{coll}(T_0) = 9$  MeV.

In addition, there can arise width modifications from the dressing of the anti-/kaon cloud through in-medium  $\phi \rightarrow K\bar{K}$  decays. Here even small effects in the kaon propagators can have appreciable impact on the  $\phi$  spectral function due to the proximity of the  $\phi$  mass to the two-kaon threshold (the  $p$ -wave nature of the  $\phi \rightarrow K\bar{K}$  decay further enhances this sensitivity). We assess this by evaluating the  $\phi \rightarrow K\bar{K}$  width in terms of in-medium modified (anti-) kaon spectral functions, *i.e.*,

$$\begin{aligned} \text{Im } \Sigma_{\phi K\bar{K}}(M; T) &= -m_\phi \Gamma_{\phi \rightarrow K\bar{K}}^{vac} \int_0^M \frac{m_1 dm_1}{\pi} A_K(m_1) \\ &\times \int_0^{M-m_1} \frac{m_2 dm_2}{\pi} A_{\bar{K}}(m_2) \left(\frac{p_K}{p_K^{on}}\right)^3 F_{\phi K\bar{K}}(p_K)^2 [1 + f^K(\omega_1) + f^{\bar{K}}(\omega_2)] \end{aligned} \quad (15)$$

( $\Gamma_{\phi \rightarrow K\bar{K}}^{vac} = 3.7$  MeV: on-shell width in free space), and again neglect possible modifications of the real part. The (anti-) kaon spectral functions are given by

$$A_{K,\bar{K}}(m) = -2 \text{Im} D_{K,\bar{K}}(m) = -2 \text{Im} \frac{1}{m^2 - m_K^2 - \Sigma_{K,\bar{K}}} . \quad (16)$$

For the finite-temperature part of  $\Sigma_{K,\bar{K}}$ , which does not distinguish between kaons and antikaons, we approximate the results of ref. [19] as

$$\begin{aligned} \text{Im} \Sigma_{K,\bar{K}}(T) &\simeq -m_K \Gamma_{K,\bar{K}}(T) = -m_K (20 \text{MeV}) \left(\frac{T}{T_0}\right)^3 \\ \text{Re} \Sigma_{K,\bar{K}}(T) &\simeq -m_K (10 \text{MeV}) . \end{aligned} \quad (17)$$

In nuclear matter kaons and antikaons behave quite differently. The  $KN$  interaction is rather weak and slightly repulsive. A corresponding selfenergy has been extracted as [33,35]

---

<sup>1</sup>This behavior is quite contrary to the light quark states  $\rho$  and  $\omega$ . The reason for that is presumably related to the OZI rule: whereas in a  $\rho$ -/ $\omega$ - $N$  interaction the antiquark in the vector meson can easily annihilate and convert into excitation energy of a baryonic resonances, the equivalent mechanism for the antistrange quark in a  $\phi$ - $N$  interaction is strongly suppressed.

$$\Sigma_K(\varrho_N) \simeq m_K (0.13m_K) \left( \frac{\varrho_N}{\varrho_0} \right) . \quad (18)$$

The antikaon, on the other hand, couples to a number of hyperon excitations. A detailed recent coupled channel calculation [34] predicts an appreciable  $\bar{K}$  width of up to 100 MeV already at nuclear saturation density, together with significant attraction as well. Accordingly, we employ

$$\Sigma_{\bar{K}}(m; \varrho_N) \simeq m_K \left( \frac{\varrho_N}{\varrho_0} \right) (-60, -i 90) \text{MeV} . \quad (19)$$

Notice that the situation reverses for the interaction with antinucleons, *i.e.*,

$$\Sigma_K(\varrho_{\bar{N}}) = \Sigma_{\bar{K}}(\varrho_N) \quad (20)$$

$$\Sigma_K(\varrho_N) = \Sigma_{\bar{K}}(\varrho_{\bar{N}}) \quad (21)$$

Thus, for central rapidities at RHIC, where the *net* baryon density in the hadronic phase is small, the combined contributions to the real part of both the anti-/kaon selfenergies practically vanish. This is not the case for the imaginary parts which will be explicitly included.

Finally, we take into account the 13% branching ratio of the free  $\phi$  decay into  $\pi\rho$ , and treat medium modifications thereof in analogy to the  $\omega \rightarrow \rho\pi$  decay, eq. (7).

Combining all contributions yields an in-medium  $\phi$  propagator of the form

$$D_\phi = [M^2 - m_\phi^2 - \Sigma_{\phi K\bar{K}} - \Sigma_{\phi\rho\pi} - \Sigma_\phi^{coll}]^{-1} . \quad (22)$$

#### 4. Spectral Functions

Fig. 1 summarizes the appearance of the light vector-meson spectral functions (=imaginary part of the propagators) that will be employed in the calculation of dilepton spectra below: both light quark states  $\rho$  and  $\omega$  undergo a strong broadening towards the expected phase boundary (one also observes a slight upward mass shift caused by repulsive parts in the selfenergy which are mainly due to baryonic particle-hole excitations [24,30], as well as medium effects in the pion tadpole graph in case of the  $\rho$  [36]). The  $\phi$  seems to retain more of its resonance structure, although, at the highest temperature, the hadronic rescattering has increased its vacuum width by over a factor of 7 to  $\sim 32$  MeV.

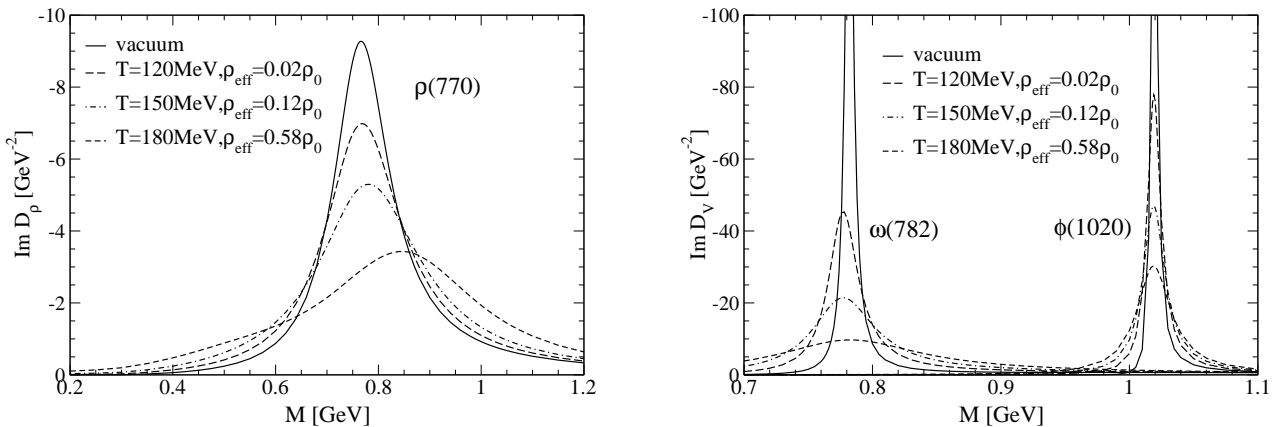


FIG. 1. Spectral functions of the light vector mesons  $\rho$  (left panel) and  $\omega, \phi$  (right panel) in vacuum (solid lines) as well as in hot baryon-poor hadronic matter as expected under RHIC conditions:  $(T, \mu_N) = (120, 91)$  MeV (long-dashed lines),  $(T, \mu_N) = (150, 40)$  MeV (dashed-dotted lines) and  $(T, \mu_N) = (180, 27)$  MeV (short-dashed lines). For the definition of  $\varrho_{eff}$  see eq. (12).

It is interesting to note that at  $T = 180$  MeV, where for the chosen value of  $\mu_B = 27$  MeV the *net* baryon density amounts to only  $0.14\rho_0$ , the combined effect of baryons and antibaryons causes an appreciable further broadening of both the  $\rho$  and  $\omega$  spectral functions as compared to the pure meson gas results, see fig. 2. This does not apply for the  $\phi$  meson. It would be very illuminating to scrutinize these features with high resolution/statistics experiments in more baryon-dominated systems as created in fixed target heavy-ion collisions.

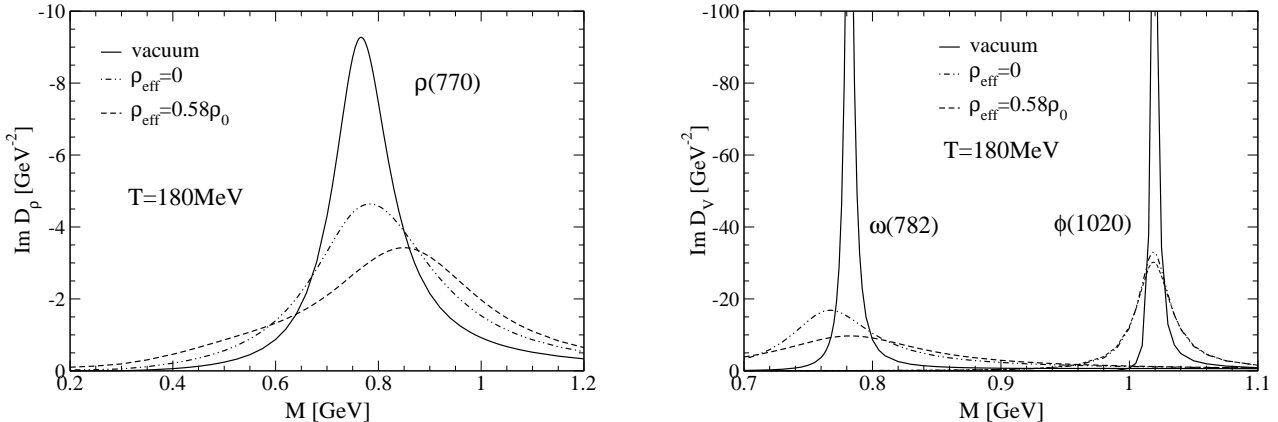


FIG. 2.  $\rho$  (left panel) and  $\omega, \phi$  (right panel) spectral functions at  $T = 180$  MeV with (short-dashed lines,  $\mu_B = 27$  MeV) and without (dashed-double-dotted lines) the effects of anti-/baryons as expected for central rapidities at RHIC.

### C. Intermediate Mass Region (IMR)

The nonperturbative mechanisms related to the deconfinement/chiral restoration transition necessarily imply substantial medium effects for the light hadronic bound states, as discussed in the previous section. Beyond invariant masses of  $M \simeq 1.5$  GeV, however, the interactions in the free vector correlator essentially become perturbative, cf. eq. (2). Naively, one might anticipate in-medium corrections to be of order  $\alpha_s$  or  $\mathcal{O}(T/M)$ ,  $\mathcal{O}(\mu_q/M)$ , but theoretically the impact of 'soft' corrections to the finite-temperature  $q\bar{q}$  rates is not very well under control, see, *e.g.*, refs. [39–42]. For the (closely related) Drell-Yan annihilation process, corrections of similar nature are subsumed in the famous  $K$ -factors, which, for modern parton distribution functions (*e.g.*, GRV-94 [43]), are around 1.3–1.5. This should roughly reflect the uncertainty when employing the lowest-order thermal  $q\bar{q} \rightarrow l^+l^-$  annihilation for the QGP phase as done below (and might be considered as a lower limit of the true emissivity). Making furthermore use of 'duality' arguments [47,5,53] we will in fact apply the corresponding dilepton production rate [45],

$$\frac{d^8 N_{\mu\mu}}{d^4 x d^4 q} = \frac{\alpha^2}{4\pi^4} \frac{T}{q} f^B(q_0; T) \sum_q e_q^2 \ln \frac{(x_- + y)(x_+ + \exp[-\mu_q/T])}{(x_+ + y)(x_- + \exp[-\mu_q/T])} \quad (23)$$

also in the hadronic phase, extrapolating it down to masses of about 1.1 GeV. The latter is motivated by the observation that lowest-order in temperature effects [46] already amount to a reduction of the 'duality threshold' towards the  $\phi$  resonance (*see, e.g.*, the discussion in [37,5]).

### D. Thermal Rates

In fig. 3 we compare the 3-momentum integrated dilepton production rates in thermal equilibrium,

$$\frac{dR_{ee}}{dM^2} = \int \frac{d^3 q}{2q_0} \frac{dR_{ee}}{d^4 q} \quad (24)$$

at fixed temperature and density for 3 different ways of evaluating the electromagnetic correlator: using hadronic degrees of freedom with (solid line) or without (dashed lines) medium effects in the vector-meson spectral functions, as well as perturbative quark-antiquark annihilation (dashed-dotted lines).

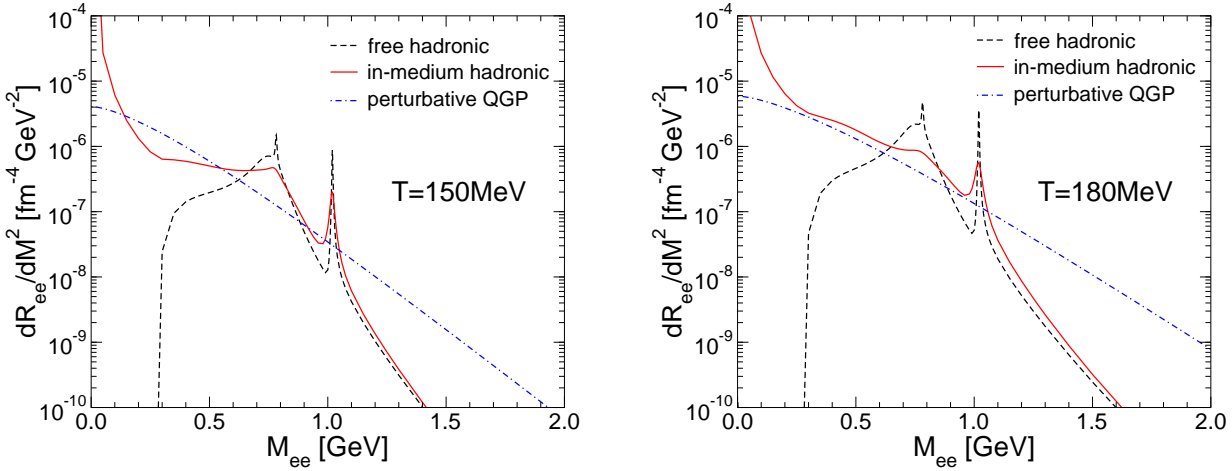


FIG. 3. 3-momentum integrated thermal dilepton production rates as appropriate for the hadronic phase at RHIC (left panel:  $(T, \mu_N) = (150, 60)$  MeV, right panel:  $(T, \mu_N) = (180, 27)$  MeV). The dashed lines are obtained when using the free  $\rho$ ,  $\omega$  and  $\phi$  spectral functions, whereas the full lines follow upon inclusion of hadronic medium effects as described in the previous section; the dashed-dotted is the result for lowest order  $\alpha_s$  quark-antiquark annihilation.

The hadronic calculations have built in contributions from 2- and 3-pion as well as  $K\bar{K}$  states through the  $\rho$  and  $\omega$  as well as the  $\phi$ , respectively. These are sufficient to saturate the strength in the electromagnetic correlator from the two-pion threshold up to about 1 GeV. Beyond, 4-pion states start to become dominant, most notably through  $\pi a_1$  and  $\pi\omega$  annihilation [38], which are rather structureless and merge into the aforementioned quark-hadron duality from  $M_{\text{dual}} \geq 1.5$  GeV on (in vacuum).

The medium effects in the spectral functions are directly reflected in the dilepton rates. The thermal Bose factor in the latter augments the enhancement on the low-mass side of the resonances (a factor of 3-10 over the free case around invariant masses  $M \simeq 0.4$  GeV for  $T = 150 - 180$  MeV). To a large extent, the underlying processes can be associated with (in matter) Dalitz decays  $\omega, a_1(1260) \rightarrow \pi e^+ e^-$  or  $N^* \rightarrow Ne^+ e^-$ , being proportional to the imaginary parts of the vector-meson selfenergies. At the same time, a strong broadening of the resonance structures is implied as a result of resumming the large imaginary parts [37,22] in the propagators. Taken together, both features seem to drive the hadronic in-medium curve towards perturbative  $q\bar{q}$  annihilation: at  $T = 180$  MeV the magnitude and slope of the former in the  $M \simeq 0.5$  GeV region are quite reminiscent to the plasma rate (not so at  $T = 150$  MeV); even in the  $\omega$  resonance region, where the maximum of the free rate is suppressed by a factor of  $\sim 6$ , the in-medium hadronic and the  $\bar{q}q$  result agree within a factor of 2. On the other hand, at  $T = 150$  MeV where the in-medium suppression amounts to a factor of  $\sim 3$ , in-medium hadronic and  $\bar{q}q$  rates differ by a factor of  $\sim 4$ .

One concludes that the indications for quark-hadron duality in dilepton production close to the phase boundary, as put forward in ref. [24] for SpS conditions, also (approximately) persist in the (almost) net baryon-free regime at RHIC.

### E. 'Background' Sources

To be able to extract information on thermal dilepton radiation in the complicated environment of heavy-ion reactions a reliable assessment of the multiple other sources is mandatory. At low masses these are mostly Dalitz decays of  $\pi^0$ ,  $\eta$  and  $\omega$  mesons as well as the direct decays of produced  $\omega$ 's and  $\phi$ 's in the final state (commonly denoted as 'hadronic cocktail'). Restricting ourselves to invariant masses above 0.5 GeV, we explicitly compute the latter two contributions based on the  $\omega$ - and  $\phi$ -abundances as obtained from the thermal fireball model at thermal break-up,

$$\frac{dN_{V \rightarrow ee}^{cktl}}{dM} = \frac{\alpha^2}{\pi^3 M} F_V(M)^2 V_{fo} \int d^3 q f^V(q_0; T_{fo}), \quad (25)$$

Here,  $V_{fo}$  is the (final) fireball 3-volume,  $f^V$  are Bose distributions and

$$F_V(M)^2 = m_V^2 |D_V^\circ(M)|^2 \quad (26)$$

the (free) electromagnetic formfactors ( $V = \omega, \phi$ ). Note that in such a framework the contribution from  $\rho$ -mesons, due to their short lifetime ( $\tau_\rho \leq \tau_\rho^{vac} = 1.3$  fm/c), is more appropriately evaluated through a slight extension of the fireball evolution, since their medium modifications around freezeout will still be significant. The same argument holds for higher resonances in the  $M \simeq 1.5$  GeV region ( $a_1, \rho'$ , etc.), which effectively make up the dual rate, eq. (23).

For still higher masses (above  $M \geq 1.5$  GeV) the most important hadronic contribution arises from the associated semileptonic decay of charmed mesons ( $D, \bar{D} \rightarrow e^+ \nu X, e^- \bar{\nu} X$ ) which originate from primordial production of  $c\bar{c}$  pairs. A comprehensive evaluation of its features has been undertaken in ref. [9], as well as in the follow-up studies in [11,12]. We will therefore not attempt to recalculate it but include the results and arguments given in these references in the discussion of the spectra below.

Finally, at masses starting from 1 GeV (primordial) Drell-Yan (DY) annihilation constitutes an important source of dileptons. Again, a detailed computation of DY-pairs at RHIC energies has been performed in ref. [9]. We here restrict ourselves to the case of central collisions of two equal nuclei with mass number  $A$ ,

$$\frac{dN_{DY}^{AA}}{dMdy}(b=0) = \frac{3}{4\pi R_0^2} A^{4/3} \frac{d\sigma_{DY}^{NN}}{dMdy}, \quad (27)$$

in terms of the (standard) elementary Drell-Yan cross section in a nucleon-nucleon collision,

$$\frac{d\sigma_{DY}^{NN}}{dMdy} = K \frac{8\pi\alpha^2}{9sM} \sum_{q=u,d,s} e_q^2 [q(x_1)\bar{q}(x_2) + \bar{q}(x_1)q(x_2)]. \quad (28)$$

The (anti-) quark distribution functions  $q(x_{1,2})$  ( $\bar{q}(x_{1,2})$ ) are taken from the leading order (LO) GRV-94 parameterization [43] (including explicit isospin asymmetries) in connection with a  $K$ -factor of 1.5 extracted from  $p$ - $A$  data [44]. Their arguments are related to the center-of-mass rapidity  $y$  and invariant mass of the lepton pair as  $x_{1,2} = xe^{\pm y}$  with  $x = M/\sqrt{s}$ , where  $s$  denotes the total *cms* energy of the nucleon-nucleon collision. In eq. (27), the root-mean-square radius parameter  $R_0 \simeq 1.05$  fm arises from a folding over a Gaussian thickness function [48]. For (slightly) off-central collisions as considered below we simply replace  $A$  in eq. (27) by the number of participants. Effects of nuclear shadowing have been estimated to reduce the total DY-yield in the RHIC regime by 20-50% [9], which is within a similar uncertainty as implicit in the thermal production rate, eq. (23).

### III. DILEPTON PRODUCTION FOR $M=0.5-3$ GEV AT RHIC

#### A. Thermal Fireball Model

The total dilepton yield from thermal radiation in a heavy-ion collision obviously depends on the space-time history of the system, which the thermal rates have to be integrated over. Here we employ a simplified thermal fireball description including, however, the most important features of a full hydrodynamic simulation in a transparent way. Assuming a spatially averaged (isotropic) temperature-density profile at each time incident, the time- and momentum-integrated thermal mass spectrum can be written as

$$\frac{dN_{ee}^{th}}{dM} = \int_0^{t_{fo}} dt V_{FC}(t) \int \frac{Md^3q}{q_0} \frac{dR_{ee}}{d^4q} [M, \vec{q}; T(t), \mu_\pi(t), \mu_B(t)] \text{Acc}(M, \vec{q}; y_0). \quad (29)$$

Experimental acceptance corrections are encoded in the factor  $\text{Acc}(M, \vec{q}; y_0)$ , which is prescribed by the specific detector characteristics, and depends on the kinematics of the produced pair as well as the rapidity positioning of the thermal fireball ( $y_0 = 0$  at RHIC). The latter has to be chosen in accord with measured hadronic rapidity distributions. As thermal fireballs typically imply smaller spreads in particle rapidity than found in heavy-ion reactions at ultrarelativistic energies [49], multiple fireballs have to be used. At the full SpS energy, *e.g.*, the full-width-half-maximum of negatives,  $dN_{h-}/dy$ , amounts to about  $\Gamma_y^{\text{SpS}} \simeq 4$ . For thermal pion distributions at the relevant temperatures one has  $\Gamma_y^{th} \simeq 1.5 - 2$ , so that two fireballs are minimally required for SpS conditions, see, *e.g.*, ref. [24]. At RHIC energies, a larger number would be necessary for a complete description. However, since our focus here is on a comparably small window around midrapidity ( $\Delta y = \pm 0.35$  as covered by the two electron arms of the PHENIX detector), a single fireball suffices. The time-dependent volume is modeled by a cylindrical expansion as

$$V_{FC}(t) = (z_0 + v_z t) \pi (r_0 + \frac{1}{2} a_\perp t^2)^2 , \quad (30)$$

where  $r_0$  is the initial transverse overlap of the two colliding nuclei (determined by the impact parameter  $b$ ),  $v_z = c$  the longitudinal expansion velocity (reflecting the approximate rapidity coverage), and  $a_\perp = 0.03 \text{ fm}^2/c^3$  is chosen to give a final transverse flow velocity of  $v_\perp \simeq 0.6c$  in connection with a typical freezeout time of  $t_{fo} \simeq 20 \text{ fm}/c$ . The largest sensitivity of our results is attached to the initial longitudinal size  $z_0$  being equivalent to a formation time (or initial temperature), which will be explicitly addressed below.

### 1. Hadronic Phase

To determine the thermodynamics of the fireball we employ the picture of subsequent chemical and thermal freezeout, which has proven very successful in describing many observables in heavy-ion collisions over a wide range of energies (from SIS to SpS), such as particle multiplicities [50,51], flow, HBT radii, etc.. From the chemical freezeout point on the composition of hadrons which are stable on the time scale of the fireball lifetime does no longer change. In systems with relatively low baryon content (SpS and RHIC) it practically coincides with the critical temperature of the chiral/deconfinement transition. Thus, for RHIC we fix it at  $T_{ch} \equiv T_c \simeq 180 \text{ MeV}$ . The two necessary input numbers are then the rapidity densities of charged particles and *net* baryons; dynamical models suggest, *e.g.*,  $dN_{ch}/dy \simeq 800$  and  $dN_B^{net}/dy \simeq 20$  at midrapidity for the full RHIC energy of  $\sqrt{s} = 200 \text{ AGeV}$  [16] (the charged particle multiplicity is in line with a naive extrapolation based on first RHIC measurements at lower energies [52]). With a standard hadronic resonance gas equation of state (EoS) these numbers imply an entropy per baryon of  $s/\varrho_B^{net} = 250$ , corresponding to a baryon chemical potential of  $\mu_B^{ch} = 27 \text{ MeV}$  at  $T_{ch}$ . Isentropic expansion (*i.e.*, at constant  $s/\varrho_B^{net}$ ) then governs the evolution of  $(T, \mu_B)$  towards thermal (kinetic) freezeout, cf. left panel of fig. 4. Since pion and kaon numbers are, by definition, also conserved, pertinent (effective) chemical potentials  $\mu_\pi$  and  $\mu_K$  are simultaneously incorporated. As opposed to SpS conditions, their values at thermal freezeout for RHIC are quite small reaching  $\mu_\pi^{th} \simeq 10 \text{ MeV}$ ,  $\mu_K^{th} \simeq 35 \text{ MeV}$  at  $T_{th} \simeq 130 \text{ MeV}$ <sup>2</sup>. Nevertheless, we include their enhancement effect in the thermal dilepton production rate from the hadronic phase as well as in the cocktail contribution, eq. (25), via

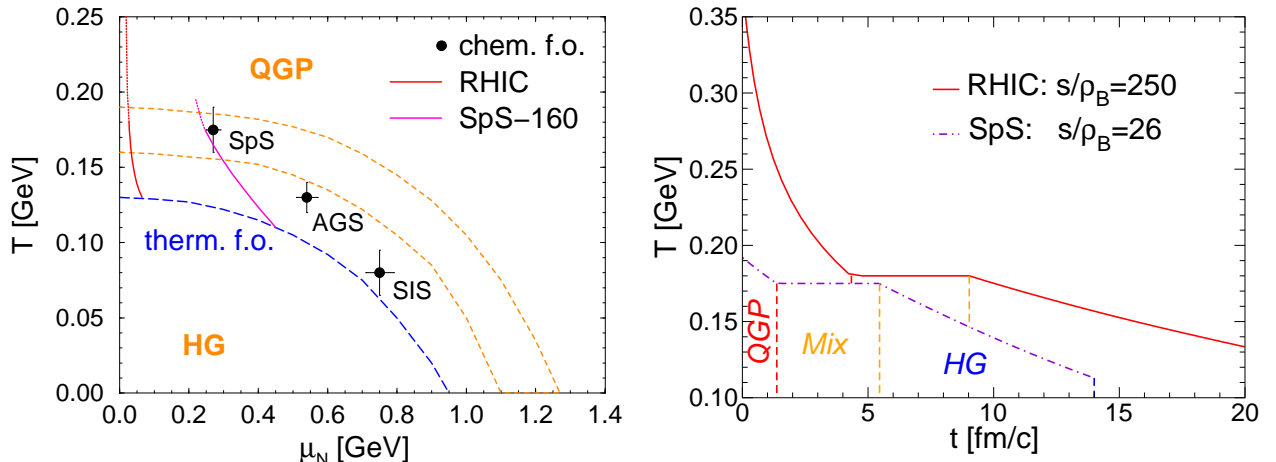


FIG. 4. Thermal fireball model description of central heavy-ion collision at SPS and RHIC energies; left panel: Thermo-dynamic trajectories for isentropic expansion in the temperature and nucleon-chemical-potential plane with additional  $\pi$ - and  $K$ -number conservation in the hadronic phases; the short-dashed lines enclose a conjectured region for the phase boundary between hadronic and quark-gluon matter, the long-dashed line represents an estimate for the thermal (kinetic) decoupling conditions in heavy-ion reactions, and the dots are the chemical freezeout points as extracted in a thermal model analysis for fixed target experiments at the SpS (160 AGeV) [50], AGS (11 AGeV) [50] and SIS (2 AGeV) [51]; right panel: time-projected temperature evolution from the formation time to thermal freezeout for central Au+Au (Pb+Pb) collisions at RHIC (SpS).

<sup>2</sup>The reason for that is the larger number of baryonic resonances at SpS, which serve as a storage of pion-number in the earlier stages, being released into pionic degrees of freedom towards thermal freezeout.

additional fugacity factors, which are  $z_\pi^2$  for  $\rho$  decays,  $z_\pi^3$  for  $\omega$  decays,  $z_K^2$  for  $\phi$  decays, and  $z_\pi^4$  in the IMR corresponding to  $\pi a_1$  and  $\pi\omega$  annihilation ( $z_x = \exp[\mu_x/T]$ ).

We finally quote the total and net baryon densities at chemical freezeout for the fireball evolutions shown in Fig. 4: at RHIC one has  $\varrho_{B,ch}^{net} = 0.14\varrho_0$  and  $\varrho_{B,ch}^{tot} = 0.54\varrho_0$ , whereas at SpS  $\varrho_{B,ch}^{tot} = 1.5\varrho_0$  and  $\varrho_{B,ch}^{net} = 1.41\varrho_0$ .

## 2. Quark-Gluon Plasma and Mixed Phase

For the early stages (starting at the formation time  $\tau_0$ ) we assume an ideal QGP EoS characterized by an entropy density

$$s_{QGP} = d_{QG} \frac{4\pi^2}{90} T^3 \quad (31)$$

(with a quark-gluon degeneracy  $d_{QG} = 16 + 10.5N_f$  and  $N_f = 2.5$ ), ignoring effects from a net baryon number ( $\mu_q \ll T$ ). Since most of the entropy is presumably produced in the pre-equilibrium stages of a collision with little changes once thermal equilibrium is established [54], we can extrapolate from the chemical freezeout backward into the QGP phase using isentropes as before. At  $T_c$ , the fraction  $f$  of matter in the hadronic phase can be inferred from the standard entropy balance

$$f s_{HG}(T_c) + (1 - f) s_{QGP}(T_c) = S_{tot}/V_{FC}(t) , \quad (32)$$

while for  $s(t) = S_{tot}/V_{FC}(t) > s_{QGP}(T_c)$  the entire system is in the plasma phase.

At collider energies (RHIC and LHC) gluons are expected to play the dominant role in early entropy production and equilibration processes [56], due to both their larger color charge as well as the steep increase of their structure functions towards low (Bjorken-)  $x$ . Although thermal equilibration seems to be achieved at a formation time of well below 1 fm/c, the chemical abundances of gluons and especially (anti-) quarks are likely to be strongly *under-saturated*. *E.g.*, in the 'self-screened parton cascade' model (SSPC) the initial parton fugacities at the thermal formation time  $\tau_0 = 0.25$  fm/c amount to  $\lambda_g(\tau_0) = n_g(T_0)/n_g^{eq}(T_0) = 0.34$  and  $\lambda_{q,\bar{q}}(\tau_0) = n_{q,\bar{q}}(T_0)/n_{q,\bar{q}}^{eq}(T_0) = 0.064$  [55] (estimates based on perturbative QCD are even lower, see, *e.g.*, [57]). To study the impact of such a scenario on the dilepton radiation from the plasma, we employ the results of ref. [54], where the SSPC initial conditions have been evolved using hydrodynamic rate equations until the onset of hadronization. For our purposes we parameterize the time dependence of the fugacities as found there by

$$\lambda_g(\tau) = 0.48 \tau^{0.26} \quad (33)$$

$$\lambda_{q,\bar{q}}(\tau) = 0.145 \tau^{0.88} + 0.02 \quad (34)$$

( $\tau$  in [fm/c]), cf. fig. 5.

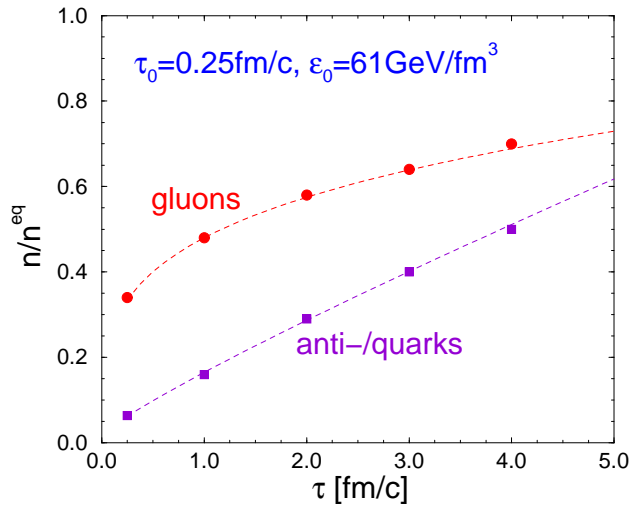


FIG. 5. Time evolution of anti-/quark (squares) and gluon (dots) fugacities as computed in a hydrodynamic simulation [54] based on initial conditions obtained from a parton cascade model [55]. The dashed lines show the results of the analytic fit, eqs. (33) and (34).

Entropy production after  $\tau_0$  was found to be on the 10% level which will be neglected here. Thus we can calculate the temperature (needed for the dilepton production rate) from the entropy density via

$$\begin{aligned} s_{QGP}^{off}(t) &= [16\lambda_g(t) + 10.5N_f\lambda_q(t)] \frac{4\pi^2}{90} T^3 \\ &\equiv d_{QG}(t) \frac{4\pi^2}{90} T^3. \end{aligned} \quad (35)$$

Since chemical equilibration is not attained before entering the mixed phase, the construction of the latter has to be modified. We assume its onset to be determined by the same critical entropy density as in the equilibrium scenario so that the critical temperature

$$T_c^{QGP}(t) = \left[ \frac{90 s_{QGP}^c}{4 d_{QG}(t) \pi^2} \right]^{1/3} \quad (36)$$

acquires a time dependence while for the hadron gas  $T_c^{HG} = 180$  MeV is kept fixed. Eq. (32) still serves to obtain the volume fraction of the hadron gas,  $f(t)$ .

As a consequence of the quark-undersaturation, the equilibrium dilepton production rate from  $q\bar{q}$  annihilation, eq. (23), is (approximately) proportional to a fugacity factor  $\lambda_q\lambda_{\bar{q}}$ , which translates into a strong suppression of the thermal yield. However, if the same initial entropy density is created as in the equilibrium scenario (which largely governs the finally observed number of secondaries), this suppression will be (partially) compensated by higher temperatures in the thermal Bose factor of the virtual photon [7]. Also, if the gluon fugacities are substantially larger than the anti-/quark ones,  $\alpha_s$ -corrections to the  $q\bar{q}$  rate become relatively more important, *e.g.*, through the process  $qg \rightarrow qee$ . As shown in ref. [15] related contributions are comparable to  $q\bar{q}$  production in a more extreme scenario of undersaturation with  $\lambda_g/\lambda_q \simeq 10$ . Since in our case  $\lambda_g/\lambda_q < 3$  after  $\tau = 1$  fm/c (and quickly decreasing further), we keep ignoring  $\alpha_s$ -corrections (as done for the equilibrium case) being aware of possibly underestimating the thermal yield from the off-equilibrium plasma by a few tens of percent.

## B. Dilepton Spectra

Let us now turn to the results for the space-time integrated dilepton spectra in central Au+Au collision at  $\sqrt{s} = 200$  AGeV. Our standard parameter set for the volume expansion within the thermal fireball model, eq. (30), is chosen as  $v_z = c$ ,  $r_0 = 6.5$  fm (reflecting an impact parameter  $b \simeq 1$  fm),  $a_{\perp} = 0.03$  fm $^2/c^3$  as well as initial longitudinal size  $z_0 = 0.6$  fm (translating into an initial temperature of  $T_0 = 370$  MeV for a chemically equilibrated QGP) and total fireball lifetime of  $t_{fo} = 20$  fm/c (resulting in a thermal freezeout temperature of  $T_{th} = 133$  MeV<sup>3</sup>).

We first focus on the LMR, cf. fig. 6. Only lepton pairs which fall into the rapidity range  $-0.35 < y < 0.35$  are included, integrated over all transverse momenta. The main significance of in-medium effects in the radiation from the thermal fireball (left panel of fig. 6) are a (strong) suppression of the yield in the  $\rho$ -omega region and an enhancement below  $M=0.65$  GeV as well as above 0.85 GeV. The  $\phi$ , on the other hand, survives as a pronounced, albeit broadened, resonance structure. These features become less distinct once the 'cocktail' contribution (from  $\omega$  and  $\phi$  decays) and the smooth yield from the QGP (which constitutes around  $\sim 20\%$ ) are added. Between  $M = 0.7$  GeV and 0.8 GeV one still observes an appreciable  $\sim 50\%$  reduction caused by in-medium effects (and a factor  $\geq 2$  enhancement towards  $M = 0.5$  GeV). Experimentally it might be even possible to subtract the 8 MeV wide contribution of free  $\omega$  decays and then try to extract a remaining structure of  $\sim 50$  MeV width – originating from  $\omega$  decays within the interacting fireball – which is still well below the free  $\rho$  width. In the  $\phi$  region our results suggest that such a procedure is less promising to succeed. The factor of 2 increase just below 1 GeV might be more easy to identify.

---

<sup>3</sup>note that this value is about 10-15% larger than at SpS energies owing to the substantially smaller baryon content at RHIC

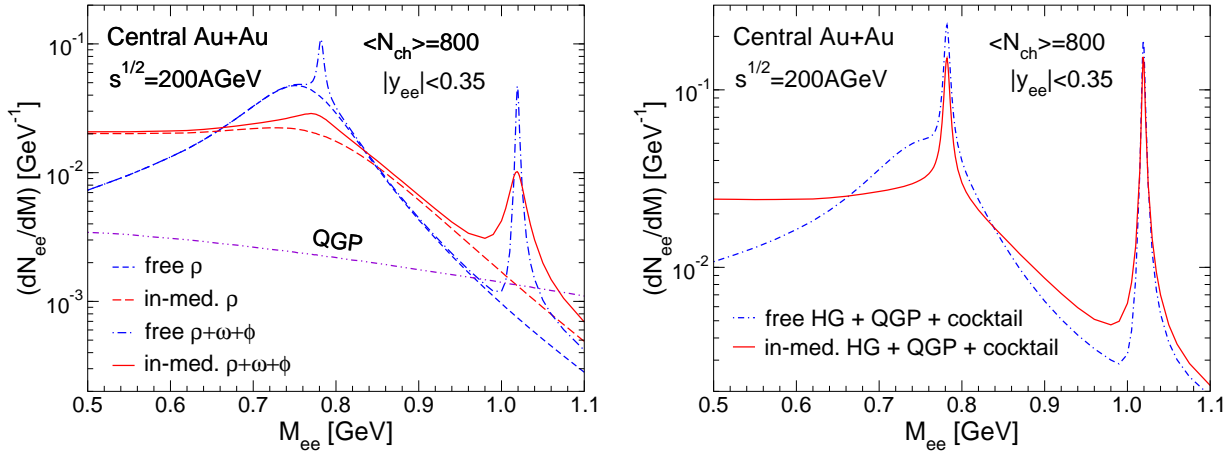


FIG. 6. Low-mass dilepton spectra around midrapidity in  $b = 1$  fm Au+Au collisions at RHIC energies. Left panel: thermal radiation from vector-meson decays in the hadronic phase with and without medium effects in the pertinent spectral functions, as well as from perturbative  $q\bar{q}$  annihilation in the plasma phase (dashed-double-dotted line). Right panel: combined yields from the hadronic and plasma phase as well as from  $\omega, \phi \rightarrow ee$  decays after freezeout; full and dashed-dotted lines correspond to the calculation with and without medium modifications, respectively, in the  $\rho, \omega$  and  $\phi$  spectral functions.

Next, we move to the IMR, first assuming QGP formation and evolution in full chemical equilibrium, cf. fig. 7. From the left panel one sees that the hadron gas radiation prevails until  $M \simeq 1.5$  GeV before the thermal radiation from the QGP phase takes over due to its smaller slope parameter (originating from larger temperatures). The QGP signal continues to outshine the (primordial) Drell-Yan yield up to about  $M \simeq 3$  GeV (similar features have been found in refs. [59,45]). Taken together, the total sum exhibits a noticeable change in slope between 1 and 4 GeV.

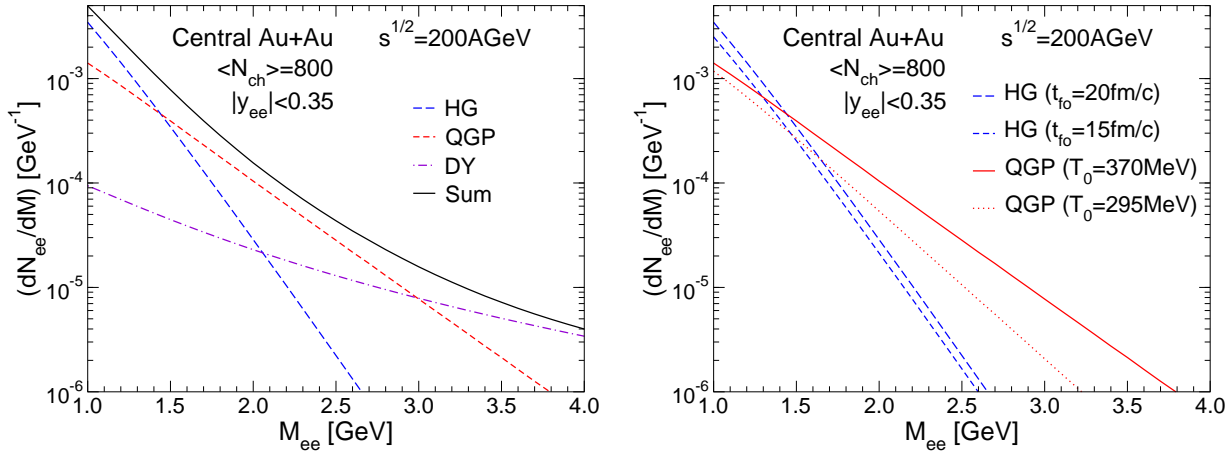


FIG. 7. Intermediate-mass dilepton spectra at RHIC energies around midrapidity assuming a chemically equilibrated QGP throughout its lifetime. Left panel: Decomposition of the thermal fireball radiation (with  $T_0 = 370$  MeV,  $t_{fo} = 20$  fm/c) into QGP (short-dashed line) and hadron gas (long-dashed lines) parts (including their respective yields from the mixed phase), compared to Drell-Yan annihilation (dashed-dotted line) and the total sum (note that open charm decays are not accounted for). Right panel: Influence of the initial temperature and fireball lifetime on the plasma and hadron gas radiation, respectively.

Not included in fig. 7 are the contributions from semileptonic decays of correlated  $c\bar{c}$  pairs. Extrapolations of their production cross sections in  $pp$  collisions to Au+Au collisions at RHIC lead to rather large dilepton emission, exceeding thermal radiation estimates by up to an order of magnitude [9,14] at invariant masses  $M \simeq 2$  GeV. However, subsequent analyses [11,12,14] investigated energy-loss effects for the charm quarks when propagating through hot and dense matter [60,61]. It was shown that the (rather hard) primordial transverse momentum distributions are substantially softened, becoming essentially thermalized. Consequently, the pertinent lepton pair invariant mass spectrum is strongly depleted above  $M \simeq 2$  GeV, by about two orders of magnitude, thus dropping below the Drell-Yan yield<sup>4</sup>. In addition, one might be able to assess the correlated charm decays independently through  $e\mu$  coincidence measurements [62] or secondary vertex displacements [63].

To test the sensitivity of our results with respect to the fireball evolution we have displayed in the right panel of fig. 7 the outcome of the following two calculations: first, doubling the initial longitudinal extent (or formation time) to  $z_0 = 1.2$  fm/c (which translates into a reduction of the initial temperature to  $T_i = 295$  MeV), the QGP radiation is appreciably decreased (by  $\sim 50\%$ ). In turn, the hadron gas evolution and corresponding dilepton yield is practically identical to the  $z_0 = 0.6$  fm case. Second, doubling the transverse acceleration to  $a_\perp = 0.06$  together with a reduced lifetime of  $t_{fo} \simeq 15$  fm/c (to maintain a similar freezeout temperature of  $T_{th} \simeq 135$  MeV as before) reduces the hadron gas part accordingly (by  $\sim 25\%$ ), whereas the plasma yield is essentially unchanged. The latter can be attributed to the predominant longitudinal expansion in the early stages leaving little impact of an increased transverse acceleration on the first 5 fm/c or so. Thus, not surprisingly, the magnitude of the plasma yield is closely linked to the formation time, whereas the hadron gas yield is a rather direct measure of the lifetime the system spends in the hadronic phase.

Furthermore, we address the question to what extent chemical undersaturation of thermal quark and gluon distribution functions in the early plasma stages affects the IMR dilepton spectra. The time evolution of the fugacities (cf. fig. 5) is implemented as described in the previous section (to account for the twice larger initial pressure we also used an accordingly increased transverse acceleration). Requiring equal initial entropy densities, the off-equilibrium scenario leads to a slightly reduced (enlarged) QGP yield below (above)  $M \simeq 3$  GeV due to a harder slope caused by the higher initial temperature<sup>5</sup>, see fig. 8.

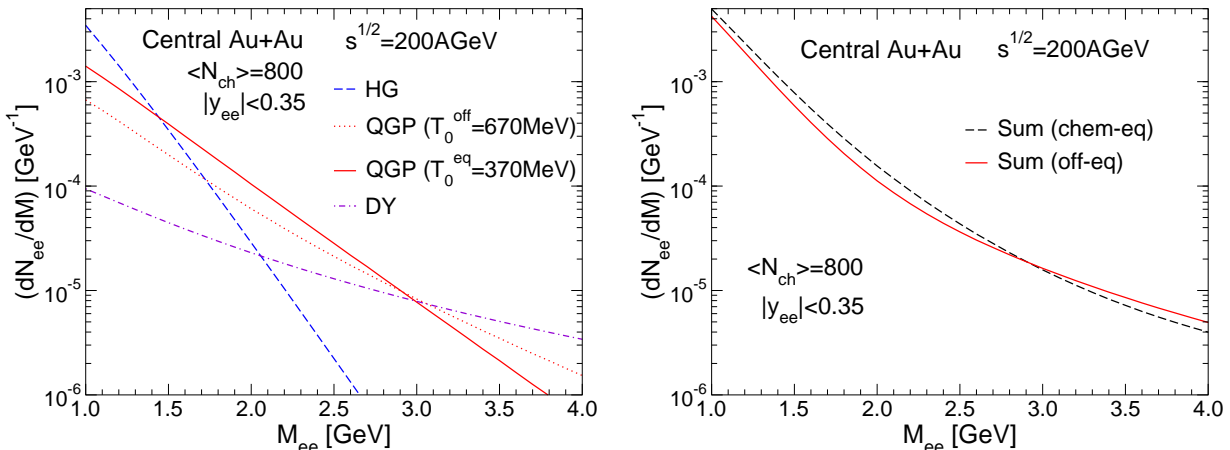


FIG. 8. Consequences of a chemically undersaturated QGP for IMR dilepton spectra at RHIC energies. Left panel: comparison of the plasma yield from a chemical equilibrium (short-dashed line) and off-equilibrium (full lines) scenario adopted from refs. [55,54] (the hadron gas contribution is virtually identical for both cases). Right panel: total sum of hadron gas, Drell-Yan and QGP contributions with (full line) and without (dashed line) chemical undersaturation in the latter.

<sup>4</sup>Most of the open charm contribution is redistributed to  $M \leq 1$  GeV; this reflects the kinematics of the two leptons emerging in randomly oriented semileptonic 3- and 4-body decays of  $c(\bar{c}) \rightarrow l^\pm \bar{\nu}(\nu) X$ , where the (thermal) charm quarks carry little kinetic energy so that  $E_l \simeq m_c/3 \simeq 0.5$  GeV.

<sup>5</sup>The small deviations from the results presented in ref. [58] arise from the fact that in there the entropy of the QGP was calculated with  $N_f = 3$  (rather than  $N_f = 2.5$  as here).

This result is a little less optimistic than the one of Shuryak and Xiong [7], who predict an enhancement of thermal IMR dilepton radiation in a similar 'hot-glue' scenario (see also ref. [65]). On the other hand, Lin and Ko, using initial conditions estimated from perturbative-QCD [64], find very strong suppression of the thermal yield which comes out well below Drell-Yan annihilation [15]. The employed initial conditions,  $\lambda_{q,0} = \lambda_{\bar{q},0} = 0.0072$ ,  $\lambda_{g,0} = 0.06$  and  $T_0 = 570$  MeV, correspond to an entropy density of  $s_0 \simeq 12 \text{ fm}^{-3}$ , which is an order of magnitude smaller than in the SSPC approach adopted here (eqs.(33), (34), and (35) give  $s_0^{\text{off}} = 122 \text{ fm}^{-3}$ ; note that for a fully equilibrated QGP at  $T = T_c \simeq 180$  MeV one has  $s = 14 \text{ fm}^{-3}$ ).

Finally, in fig. 9 we summarize the results for the combined LMR and IMR spectra with additional acceptance restrictions on the single-electron tracks as applicable for the PHENIX detector ( $p_t^e > 0.2 \text{ GeV}$ ,  $|y_e| \leq 0.35$ , opening angle  $\Theta_{ee} \geq 35$  mrad and an overall pair mass resolution of  $\sigma_M/M = 0.5 \%$ ).

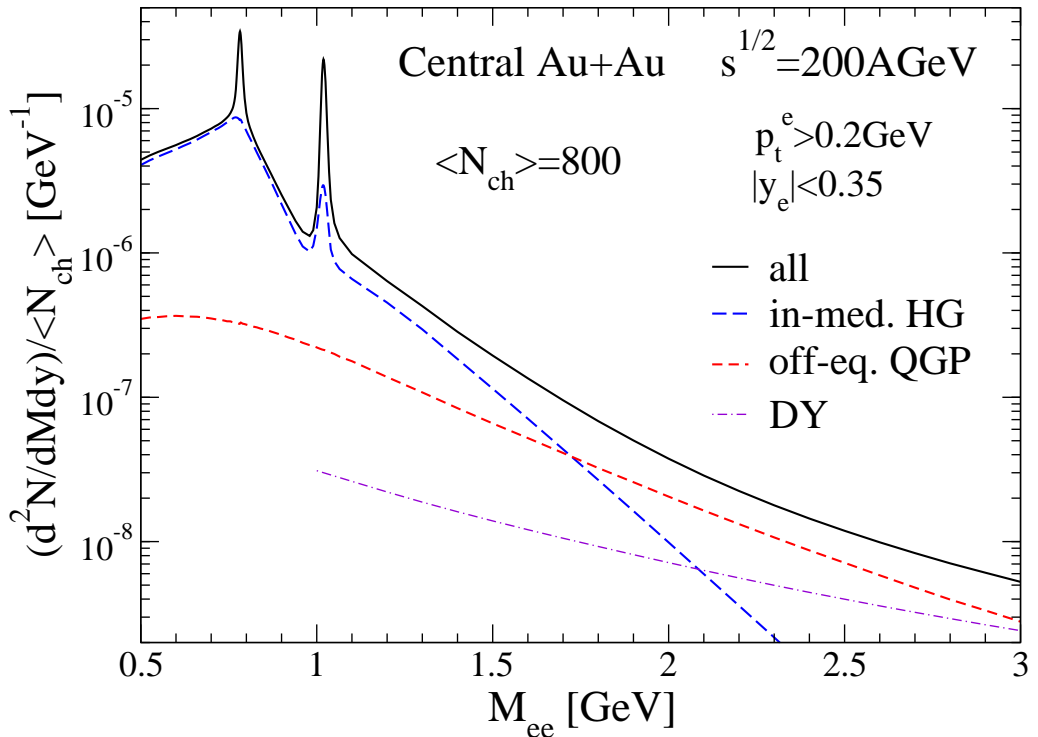


FIG. 9. Total dilepton spectrum from  $b = 1$  fm Au+Au collisions at RHIC energies around midrapidity including schematic experimental acceptance cuts appropriate for the PHENIX experiment (the  $\omega, \phi \rightarrow e^+e^-$  cocktail contributions are not separately shown but included in the solid curve). Note that semileptonic decays of correlated anti-/charm and anti-/bottom quarks have been left out.

#### IV. SUMMARY AND CONCLUSIONS

Within a thermal framework we have discussed properties of dilepton radiation from ultrarelativistic heavy-ion collisions under conditions relevant for the PHENIX experiment at RHIC.

In the first part of this article dilepton emission from static equilibrium matter has been evaluated. The emphasis was on the low-mass region ( $M \leq 1 \text{ GeV}$ ), where it was found that medium modifications of the light vector mesons induce an appreciable reshaping of the free electromagnetic current correlator. Based on standard many-body techniques, hadronic interactions in hot matter at small net-baryon content generate a strong broadening of both the  $\rho$  and  $\omega$  spectral functions. Close to  $T_c$ , the  $\omega$  width increases by almost a factor of 20 over its vacuum value, with non-negligible contributions from rescattering off thermally excited anti-/baryons. The  $\phi$  meson retains more of its resonance structure, although its free width is also augmented by up to a factor of 7-8. With that exception in

mind, the resulting in-medium hadronic dilepton production rates approach the continuum shape of lowest-order  $q\bar{q}$  annihilation to within a factor of 2 in the vicinity of the phase boundary. We have thus argued that towards  $T_c$  'quark-hadron duality' in the vector channel, which in vacuum is marked by the applicability of perturbative QCD above  $M \simeq 1.5$  GeV, extends down to rather low masses of  $\sim 0.5$  GeV (this scale is in fact comparable to typical thermal energies of free (massless) partons). These findings comply with earlier analyses that were carried out for more baryon-rich matter.

To calculate dilepton spectra for central Au+Au collisions at RHIC energies we have employed a thermal fireball model including chemical off-equilibrium effects in both the QGP and hadron gas phases. In the hadronic evolution from chemical to thermal freezeout quite moderate pion and kaon chemical potentials of 10-30 MeV emerge. The resulting low-mass dilepton yield reflects upon the lifetime of the hadronic system. As a promising signature, the final invariant-mass spectra contain a  $\sim 50$  MeV-wide structure from in-medium  $\omega$  decays. This is well below the free  $\rho$  width (150 MeV), but much larger than the width associated with free  $\omega$  decays (8.4 MeV). The latter, leading to copious dilepton production after freezeout, will mask the in-medium contribution in the measured spectra. However, with sufficiently high mass resolution as anticipated in the PHENIX experiment, the  $\omega$  'cocktail' yield should be subtractable, thus enabling access to the in-medium part.

In the intermediate-mass region the focus was on radiation from a thermalized partonic medium. Here, our investigation was of a more qualitative nature. On the one hand, this is due to uncertainties in the QGP production rate (which we might have underestimated by up to a factor of 2) as well as in the formation/composition of the 'Gluon-Quark' plasma. Nevertheless, our main point in this context should not be affected, namely that chemical undersaturation scenarios for gluons and especially anti-/quarks in the early stages do not decrease the thermal radiation in the 1.5-3 GeV region below the Drell-Yan yield – provided the production of the finally observed entropy (as encoded in produced secondaries) essentially occurs within the first fraction of a fm/c after nuclear impact (parton cascade models and hydrodynamic simulations support this assumption). On the other hand, the question remains whether the dilepton yield from correlated open charm decays can be determined accurately enough to disentangle QGP signals. A combination of experimental (*e.g.*,  $e\mu$  coincidence measurements) and theoretical efforts (*e.g.*, reliable estimates of energy loss effects in charm quark propagation) might well achieve the required sensitivity.

Finally, let us comment on further issues that are likely to be addressed with potential upgrades of the PHENIX detector (such as additional vertex tracking devices [63]). First, a direct measurement of open charm production would improve the possibilities of studying direct QGP radiation substantially. Second, an evaluation of combinatorial background could facilitate a measurement of the low-mass continuum around the vector-meson resonances, thus scrutinizing in-medium modifications of the  $\rho$  meson in a net baryon-free environment. Since the isovector ( $\rho$ ) channel has a well-defined chiral partner in form of the  $a_1$  channel, questions concerning chiral symmetry restoration can be investigated. Similar connections are less direct for  $\omega$  or  $\phi$  mesons.

## ACKNOWLEDGMENTS

I am grateful for productive conversations with A. Drees, B. Kämpfer, E.V. Shuryak, I. Tserruya and J. Wambach. This work was supported in part by the Alexander-von-Humboldt foundation (Feodor-Lynen program) and the U.S. Department of Energy under Grant No. DE-FG02-88ER40388.

---

- [1] E.V. Shuryak, Phys. Rep. **61**, 71 (1980).
- [2] G. Agakichiev *et al.*, CERES collaboration, Phys. Rev. Lett. **75**, 1272 (1995); Phys. Lett. **B422**, 405 (1998); Nucl. Phys. **A661**, 23 (1999).
- [3] N. Masera *et al.* (HELIOS-3 collaboration), Nucl. Phys. **A590**, 93c (1995); A.L.S. Angelis *et al.* (HELIOS-3 collaboration), preprint CERN-EP/98-82.
- [4] M.C. Abreu *et al.* (NA38/NA50 collaboration), preprint CERN-EP/99-112; E. Scomparin *et al.* (NA50 collaboration), J. Phys. **G25**, 235 (1999); P. Bordalo *et al.* (NA50 collaboration), Nucl. Phys. **A661**, 538 (1999).
- [5] R. Rapp and J. Wambach, hep-ph/9909229, to appear in Adv. Nucl. Phys. (2000).
- [6] J. Kapusta, L. McLerran and D.K. Srivastava, Phys. Lett. **B283**, 145 (1992).
- [7] E. Shuryak and L. Xiong, Phys. Rev. Lett. **70**, 2241 (1993).
- [8] B. Kämpfer, O.P. Pavlenko, M.I. Gorenstein, A. Peshier and G. Soff, Z. Phys. **A353**, 71 (1995).
- [9] S. Gavin, P.L. McGaughey, P.V. Ruuskanen and R. Vogt, Phys. Rev. **C54**, 2606 (1996).
- [10] M.G.-H. Mostafa, C.-Y. Wong, L. Chatterjee and Z.-Q. Wang, Int. J. Mod. Phys. **E5**, 631 (1996).

[11] E. Shuryak, Phys. Rev. **C55**, 961 (1997).

[12] Z. Lin, R. Vogt and X.-N. Wang, Phys. Rev. **C57**, 899 (1998).

[13] A.V. Leonidov and P.V. Ruuskanen, Eur. Phys. J. **C4**, 519 (1998).

[14] K. Gallmeister, B. Kämpfer and O.P. Pavlenko, Phys. Rev. **C57**, 3276 (1998); Eur. Phys. J. **C8**, 473 (1999).

[15] Z. Lin and C.M. Ko, Nucl. Phys. **A671**, 567 (2000).

[16] S. Bass *et al.*, Nucl. Phys. **A661**, 205 (1999).

[17] E.L. Feinberg, Nuovo Cim. **A34**, 391 (1976).

[18] L. McLerran and T. Toimela, Phys. Rev. **D31**, 545 (1985).

[19] E.V. Shuryak, Nucl. Phys. **A533**, 761 (1991).

[20] K. Haglin, Nucl. Phys. **A584**, 719 (1995).

[21] J. Alam, S. Sarkar, P. Roy, B. Dutta-Roy and B. Sinha, Phys. Rev. **C59**, 905 (1999).

[22] R. Rapp and C. Gale, Phys. Rev. **C60**, 024903 (1999).

[23] R. Rapp, G. Chanfray and J. Wambach, Nucl. Phys. **A617**, 472 (1997).

[24] R. Rapp and J. Wambach, Eur. Phys. J. **A6**, 415 (1999).

[25] J.J. Sakurai, Phys. Rev. Lett. **8**, 300 (1962).

[26] M. Gell-Mann, D. Sharp, and W.G. Wagner, Phys. Rev. Lett. **8**, 61 (1962).

[27] C.M. Ko and D. Seibert, Phys. Rev. **C49**, 2198 (1994).

[28] K. Haglin and C. Gale, Nucl. Phys. **B421**, 613 (1994).

[29] A. Bhattacharyya, S.K. Ghosh, S.C. Phatak, and S. Raha, Phys. Rev. **C55**, 1463 (1997).

[30] B. Friman, M. Lutz and G. Wolf, in Proc. of the Int. Workshop XXVIII on Gross Properties of Nuclei and Nuclear Excitations (Hirschegg, Austria, Jan. 16-22, 2000), edt. by M. Buballa, W. Nörenberg, B.-J. Schaefer and J. Wambach, GSI Darmstadt 2000, p. 161, and [nucl-th/0003012](#).

[31] F. Klingl, N. Kaiser and W. Weise, Nucl. Phys. **A624**, 527 (1997).

[32] R. Rapp, M. Urban, M. Buballa and J. Wambach, Phys. Lett. **B417**, 1 (1998).

[33] N. Kaiser, P.B. Siegel and W. Weise, Nucl. Phys. **A594**, 325 (1995).

[34] A. Ramos and E. Oset, Nucl. Phys. **A671**, 481 (2000).

[35] E. Oset and A. Ramos, [nucl-th/0005046](#).

[36] M. Urban, M. Buballa, R. Rapp and J. Wambach, Nucl. Phys. **A673**, 357 (2000).

[37] R. Rapp, Nucl. Phys. **A661**, 33 (1999).

[38] G.Q. Li and C. Gale, Phys. Rev. **C58**, 2914 (1998).

[39] E. Braaten, R. Pisarski and T.C. Wang, Phys. Rev. Lett. **64**, 2242 (1990).

[40] L. Chatterjee and C.-Y. Wong, Phys. Rev. **C51**, 2125 (1995).

[41] C.H. Lee, J. Wirstam, I. Zahed and T.H. Hansson, Phys. Lett. **B448**, 168 (1999).

[42] A. Peshier and M.H. Thoma, Phys. Rev. Lett. **84**, 841 (2000).

[43] M. Glück, E. Reya and A. Vogt, Z. Phys. **C67**, 433 (1995).

[44] C. Spieles *et al.*, Eur. Phys. J. **C5**, 349 (1998).

[45] J. Cleymans, J. Fingberg and K. Redlich, Phys. Rev. **D35**, 2153 (1987).

[46] M. Dey, V.L. Eletsky and B.L. Ioffe, Phys. Lett. **B252**, 620 (1990).

[47] A.V. Leonidov and P.V. Ruuskanen, Heavy Ion Phys. **1**, 61 (1995).

[48] C.-Y. Wong, Phys. Rev. **D30**, 961 (1984).

[49] J. Stachel, Nucl. Phys. **A610**, 509c (1996).

[50] P. Braun-Munzinger, J. Stachel, J.P. Wessels and N. Xu, Phys. Lett. **B344**, 43 (1994); *ibid.* **B365**, 1 (1996);  
P. Braun-Munzinger and J. Stachel, Nucl. Phys. **A638**, 3c (1998);  
P. Braun-Munzinger, I. Heppe and J. Stachel, Phys. Lett. **B465**, 15 (1999).

[51] J. Cleymans and K. Redlich, Phys. Rev. **C60**, 054908 (1999);  
J. Cleymans, H. Oeschler and K. Redlich, Phys. Rev. **C59**, 1663 (1999).

[52] B.B. Back *et al.*, PHOBOS collaboration, [hep-ex/0007036](#), and Phys. Rev. Lett. (2000), in print.

[53] R. Rapp and E. Shuryak, Phys. Lett. **473**, 13 (2000).

[54] D.M. Elliott and D.H. Rischke, Nucl. Phys. **A671**, 583 (2000).

[55] B. Müller, M.G. Mustafa and D.K. Srivastava, Heavy Ion Phys. **5**, 387 (1997).

[56] E.V. Shuryak, Phys. Rev. Lett. **68**, 3270 (1992).

[57] K.J. Eskola and K. Kajantie, Z. Phys. **C75**, 515 (1997).

[58] R. Rapp, in Proc. of the Int. Workshop XXVIII on Gross Properties of Nuclei and Nuclear Excitations (Hirschegg, Austria, Jan. 16-22, 2000), edt. by M. Buballa, W. Nörenberg, B.-J. Schaefer and J. Wambach, GSI Darmstadt 2000, p. 211, and [hep-ph/0001291](#).

[59] K. Kajantie, J. Kapusta, L. McLerran and A. Mekjian, Phys. Rev. **D34**, 2746 (1986).

[60] M. Gyulassy and X.-N. Wang, Nucl. Phys. **B420**, 583 (1994).

[61] R. Baier, Y.L. Dokshitzer, S. Peigne and D. Schiff, Phys. Lett. **B345**, 277 (1995);  
R. Baier, D. Schiff and B.G. Zakharov, [hep-ph/0002198](#), to appear in Ann. Rev. Nucl. and Part. Sci..

[62] PHENIX conceptual Design Report, 1993, unpublished; PHENIX homepage under <http://www.phenix.bnl.gov>.

- [63] I. Tserruya and A. Drees, private communication (2000).
- [64] M. Gyulassy and X.-N. Wang, *Comput. Phys. Commun.* **83**, 307 (1994);  
X.-N. Wang, *Phys. Rep.* **280**, 287 (1997).
- [65] S. Raha, *Physica Scripta* **T32**, 180 (1990).